

Time-dependent quantum wave packet simulation for strong laser-induced molecular dynamics in multiple electronic states of H_2 molecules

Jin-Peng Ma(马金鹏), Xiao-Qing Hu(胡晓青), Yong Wu(吴勇), and Jian-Guo Wang(王建国)

Citation: Chin. Phys. B, 2025, 34 (**10**): 103301. DOI: 10.1088/1674-1056/adf319
http://cpb.iphy.ac.cn; http://iopscience.iop.org/cpb

What follows is a list of articles you may be interested in

Rotational dynamics of neutral O_2 driven by linearly, elliptically and circularly polarized femtosecond pulsed lasers

Ting Xu(许婷), Jin-Peng Ma(马金鹏), Xiao-Qing Hu(胡晓青), Yin-Song Tang(唐寅淞), Si-Qi Pei(裴思琪), Cong-Cong Jia(贾聪聪), Yong-Wu(吴勇), and Jian-Guo Wang(王建国)
Chin. Phys. B, 2025, 34 (**5**): 053301. DOI: 10.1088/1674-1056/adbeea

Line positions, intensities, and Einstein *A* coefficients for 3-0 band of $^{12}C^{16}O$: A spectroscopy learning method

Zhi-Xiang Fan(范志祥), Zhi-Zhang Ni(倪志樟), Jie-Jie He(贺洁洁), Yi-Fan Wang(王一凡), Qun-Chao Fan(樊群超), Jia Fu(付佳), Yong-Gen Xu(徐勇根), Hui-Dong Li(李会东), Jie Ma(马杰), and Feng Xie(谢锋)
Chin. Phys. B, 2021, 30 (**12**): 123301. DOI: 10.1088/1674-1056/ac3069

Tracking coherent low frequency vibrational information of Rh101 in ground and excited electronic states by broadband transient grating spectroscopy

Wei Zhang(张伟), Xiao-Song Liu(刘小嵩), Zan-Hao Wang(王赞浩), Yun-Fei Song(宋云飞), Yan-Qiang Yang(杨延强)
Chin. Phys. B, 2018, 27 (**12**): 123301. DOI: 10.1088/1674-1056/27/12/123301

Photoassociation spectra of ultracold $^{85}Rb_2$ molecule in 0_u^+ long range state near the $5S_{1/2}+5P_{1/2}$ asymptote

Guodong Zhao(赵国栋), Dianqiang Su(苏殿强), Zhonghua Ji(姬中华), Tengfei Meng(孟腾飞), Yanting Zhao(赵延霆), Liantuan Xiao(肖连团), Suotang Jia(贾锁堂)
Chin. Phys. B, 2017, 26 (**8**): 083301. DOI: 10.1088/1674-1056/26/8/083301

Infrared diode laser spectroscopy of O_2–N_2O van der Waals complex in the v_1 symmetric stretch region of N_2O

Li Song (李松), Zheng Rui (郑锐), Duan Chuan-Xi (段传喜)
Chin. Phys. B, 2014, 23 (**12**): 123301. DOI: 10.1088/1674-1056/23/12/123301

SPECIAL TOPIC — Ultrafast physics in atomic, molecular and optical systems

Time-dependent quantum wave packet simulation for strong laser-induced molecular dynamics in multiple electronic states of H_2 molecules

Jin-Peng Ma(马金鹏)[1], Xiao-Qing Hu(胡晓青)[1,†], Yong Wu(吴勇)[1,2], and Jian-Guo Wang(王建国)[1]

[1] *National Key Laboratory of Computational Physics Institute of Applied Physics and Computational Mathematics, Beijing* 100088, *China*
[2] *HEDPS, Center of Applied Physics and Technology, Peking University, Beijing* 100084, *China*

(Received 26 May 2025; revised manuscript received 6 July 2025; accepted manuscript online 23 July 2025)

We present a fully time-dependent quantum wave packet evolution method for investigating molecular dynamics in intense laser fields. This approach enables the simultaneous treatment of interactions among multiple electronic states while simultaneously tracking their time-dependent electronic, vibrational, and rotational dynamics. As an illustrative example, we consider neutral H_2 molecules and simulate the laser-induced excitation dynamics of electronic and rotational states in strong laser fields, quantitatively distinguishing the respective contributions of electronic dipole transitions (within the classical-field approximation) and non-resonant Raman processes to the overall molecular dynamics. Furthermore, we precisely evaluate the relative contributions of direct tunneling ionization from the ground state and ionization following electronic excitation in the strong-field ionization of H_2. The developed methodology shows strong potential for performing high-precision theoretical simulations of electronic-vibrational-rotational state excitations, ionization, and dissociation dynamics in molecules and their ions under intense laser fields.

Keywords: time-dependent quantum wave packet evolution method, laser-induced excitation dynamics, electronic dipole transitions, non-resonant Raman processes, direct tunneling ionization, ionization following electronic excitation

PACS: 33.15.Mt, 33.20.Sn, 33.20.Wr, 32.80.–t

DOI: 10.1088/1674-1056/adf319 **CSTR:** 32038.14.CPB.adf319

1. Introduction

When intense laser fields interact with matter, such fields drive directional or periodic motion of electrons and atomic nuclei, thereby altering the state of matter.[1–4] Within the classical field approximation, this interaction can be expressed as $\boldsymbol{E}\cdot\boldsymbol{R}_i - \boldsymbol{E}\cdot\boldsymbol{r}_j$, where $\boldsymbol{R}_i$ and $\boldsymbol{r}_j$ represent the coordinates of positive and negative charges, respectively. Theoretically, solving the time-dependent Schrödinger equation that incorporates both the field and all particles enables the extraction of dynamical information such as photoexcitation,[5–7] photoionization,[8–10] molecular alignment,[11–13] and dissociation processes.[14–17] However, for molecular systems containing multiple nuclei and numerous electrons, directly solving the Schrödinger equation becomes computationally intractable. In such cases, time-dependent evolution methods employing basis functions of molecular electronic-vibrational-rotational states within the Born-Oppenheimer approximation and the interaction representation emerge as an effective approach for investigating molecular dynamics in intense laser fields.

Within the molecular framework, the interaction between intense laser fields and molecules can be expressed as $\boldsymbol{E}\cdot\boldsymbol{D}$, where $\boldsymbol{D}$ represents both the permanent dipole moments of molecular electronic states and the transition dipole moments between different electronic states. For different physical processes, two time-dependent evolution approaches have been developed to investigate molecular dynamics. The first approach addresses nonresonant Raman excitation of rotational states in neutral molecules,[18–21] where resonant electronic transitions can be neglected and only the ground electronic state is considered in the calculations. Here, the laser–molecule interaction is further approximated as $-E^2\alpha/2$, where α denotes the molecular dipole polarizability derived from quantum perturbation theory and the molecular dipole moment $\boldsymbol{D}$,[22] which fundamentally describes a second-order process involving virtual photoexcitation and subsequent de-excitation under the external field, and the contributions of all excited states are comprehensively included.[20] The second theoretical approach characterizes laser-induced resonant electronic transition processes, explicitly incorporating dipole interactions between two or several dominant electronic states and the external field.[23,24] This methodology enables investigations of single-photon transitions, multiphoton transitions, and resonant laser-driven Raman processes. A prototypical application involves studying dissociation dynamics in H_2^+ molecules through fully quantum-mechanical time-dependent

†Corresponding author. E-mail: xiaoqing-hu@foxmail.com

© 2025 Chinese Physical Society and IOP Publishing Ltd. All rights, including for text and data mining, AI training, and similar technologies, are reserved.

simulations.[25–31] These theoretical frameworks have elucidated critical mechanisms including electron-nuclear correlation dynamics during bond rupture, field-induced bond softening effects,[15,32] and electron localization phenomena[27,33] in molecular dissociation pathways.[34–38]

It is noteworthy that although these two methodologies[18–20,23,24] specifically target resonant and nonresonant laser-induced molecular dynamics, respectively, these processes inherently coexist. First, given the high density of molecular excited states, multiphoton resonance with specific states inevitably occurs under the laser field; moreover, when the laser field is sufficiently strong, electronic transitions may proceed even without strict resonance conditions. This makes a rigorous definition of purely nonresonant laser–molecule interactions fundamentally challenging. Furthermore, when external fields satisfy single- or multiphoton resonance conditions with particular electronic transitions, concurrent nonresonant Raman processes inevitably emerge with numerous other states. High-precision theoretical modeling of laser-driven molecular dynamics must inherently account for both interaction mechanisms through self-consistent frameworks. However, directly incorporating both types of interactions within a single Schrödinger equation leads to an improper theoretical formulation. This arises because the dipole polarizability α inherently encapsulates all excited-state contributions to second-order transition processes involving the ground state. Therefore, it cannot coexist with explicit excited states in the model without introducing double counting of these interactions. The simultaneous treatment of laser-induced resonant and nonresonant interactions remains one of the fundamental challenges in contemporary strong-field physics research.

In this work, we have developed a novel fully time-dependent quantum wave packet propagation methodology (TDQWPM). This framework incorporates the interactions of numerous highly excited electronic states with external fields, extending beyond conventional treatments limited to ground and low-lying excited states. These states encompass most single-electron excited configurations and multiple double-electron excited states in the ground-state molecular system. This comprehensive approach enables the simultaneous description of both resonant photonic transitions between ground and low-lying states and over 95% of nonresonant Raman excitation processes. By employing neutral H_2 molecules as a prototypical system, we have computationally investigated the laser-driven excitation dynamics involving both electronic and rotational degrees of freedom in intense laser fields. Our simulations provide quantitative insights into the distinct roles played by classical-field-approximated electronic transitions and nonresonant Raman processes in governing molecular dynamics. Moreover, we have established a precise quantification of the relative importance of direct ground-state tunneling ionization and excitation-mediated ionization pathways in the strong-field ionization of H_2. This developed methodology exhibits significant potential for achieving high-fidelity theoretical simulations of coupled electronic-vibrational-rotational excitations, ionization processes, and dissociation dynamics in molecules and molecular ions subjected to intense laser irradiation.

This paper is structured as follows. In Section 2, we provide the theoretical model of a fully time-dependent quantum wave packet evolution method for investigating molecular dynamics under strong laser fields. In Section 3, we present the numerical results and discussion of classical-field-approximated electronic transitions and nonresonant Raman processes at different wavelengths, and distinguish the alignment dependence between direct tunneling ionization from the ground state and ionization following electronic excitation. Finally, Section 4 presents the conclusions of this study.

2. Numerical method

2.1. Calculation of molecular structural parameters

In this work, 90 electronic states (30 $X^1\Sigma_g^+$ states, 30 Σ_u^+ states, and 30 Π_u states) are included in molecular structural calculations. These calculations are performed using the MOLPRO quantum chemistry software package,[39] employing the multi-reference configuration interaction (MRCI) method. This method is particularly well-suited for describing electronic correlation in systems with multiple electronic states, which is crucial for accurately describing our target molecule. Furthermore, we utilize the diffuse-augmented correlation-consistent polarized valence quadruple zeta (d-aug-cc-pVQZ) basis set,[40] a high-quality basis set that provides excellent accuracy by including diffuse functions. The potential energy curves (PECs) of various electronic states of neutral H_2 molecules, calculated using this approach, are illustrated in Fig. 1(a), providing a visual representation of the energy landscape relevant to the present study.

To verify that the inclusion of 90 electronic states is sufficient to describe dipole polarization effects, we employ quantum perturbation theory to calculate the laser-field-induced energy correction to the ground state. Accurate to second order, the corrected energy can be expressed as follows [atomic units (a.u.) $e = m = \hbar = 1$ are used hereafter unless otherwise indicated]:

$$E_0' = E_0 + \langle 0|H'|0\rangle + \sum_{n\neq 0} \frac{\langle 0|H'|n\rangle\langle n|H'|0\rangle}{E_0 - E_n}. \tag{1}$$

Here, the zeroth-order term represents the energy calculated by the *ab initio* method. The first-order term represents the permanent dipole moment; if this term is nonzero, it induces single-photon transitions within electronic states, leading to vibrational and rotational transitions. The second-order term represents polarizability, which induces nonresonant two-photon Raman transitions within electronic states.

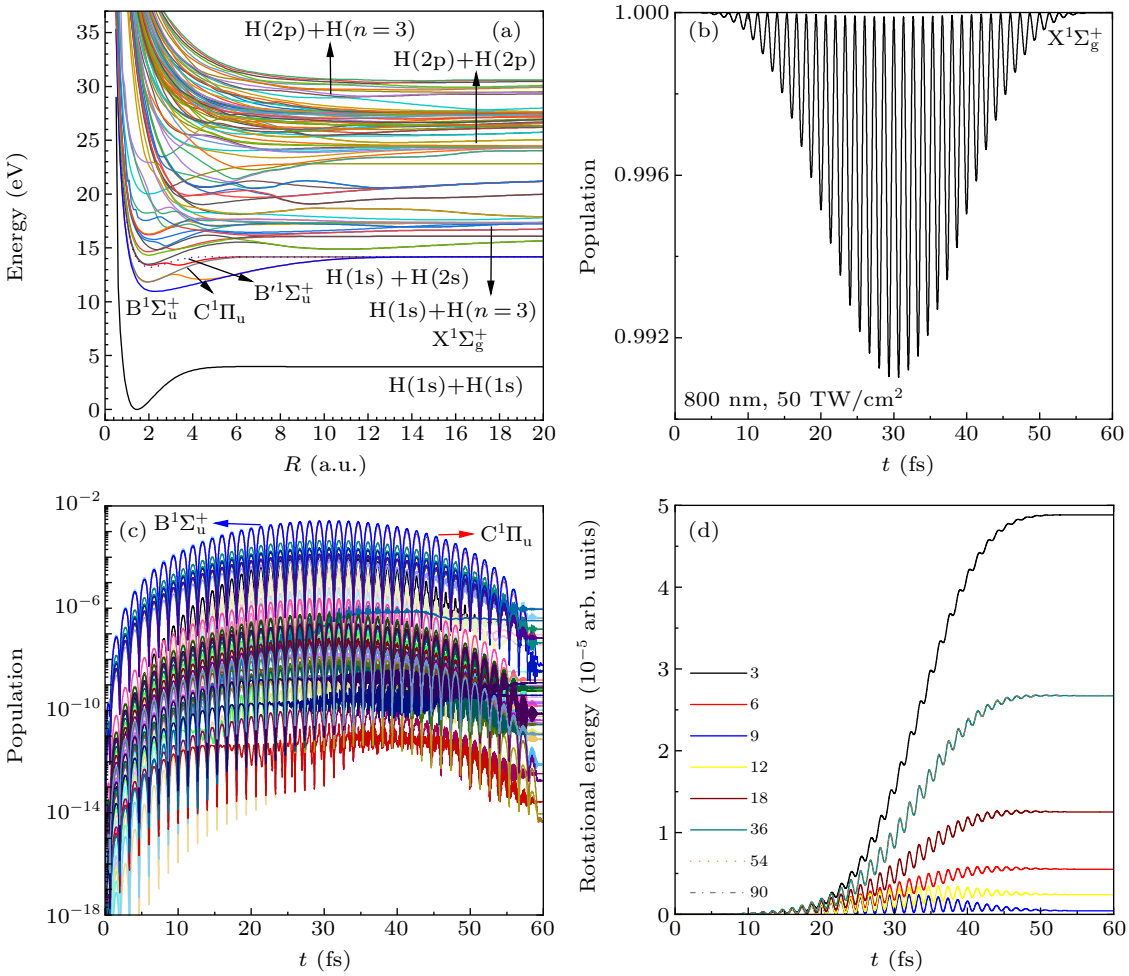


Fig. 1. (a) Potential energy curves (PECs) of the neutral H_2 molecule as a function of the internuclear distance R, including 90 electronic states. Atomic units (a.u.) are used throughout unless otherwise specified. (b) Time-dependent population of the ground state $X^1\Sigma_g^+$ under an 800 nm laser pulse with an intensity of 50 TW/cm^2. (c) Time-dependent populations of the 89 excited electronic states. Among these, the $B^1\Sigma_u^+$ (blue solid line) and $C^1\Pi_u$ (red solid line) states dominate, with minimal difference between their respective population curves. (d) Time-dependent rotational energy of the molecule considering different numbers of electronic states.

Suppose that the electric field E is applied along the z-direction. In this case, the perturbation Hamiltonian $H^{(1)}$ can be written as

$$H^{(1)} = -D_z E. \tag{2}$$

For the homonuclear diatomic molecule H_2, the intrinsic dipole moment is zero. Therefore, only the second-order term contributes to the energy correction, which can be expressed as

$$E_0' = \sum_{n\neq 0} \frac{D_{0n}^2}{E_0 - E_n} E^2. \tag{3}$$

By comparing this expression with the formula for the energy correction due to field-induced polarization, $\frac{1}{2}\alpha E^2$, we obtain

$$\alpha_{zz} = 2\sum_{n\neq 0} \frac{D_{0n}^2}{E_0 - E_n}, \tag{4}$$

where α_{zz} is the dipole polarizability calculated from the 90 electronic states. Using the same procedure, we can also obtain α_{xx} and α_{yy}.

2.2. A time-dependent quantum wave-packet evolution method

For molecules in a laser field, the Hamiltonian can be expressed as

$$\boldsymbol{H}(t) = \boldsymbol{H}_0 + \boldsymbol{H}'(t), \tag{5}$$

where $\boldsymbol{H}_0$ represents the Hamiltonian of an isolated molecule in the field-free case, and its eigenstates can be written as $|n\nu j\rangle$, where n, ν, and j label the quantum numbers of the electronic, vibrational, and rotational states, respectively. The term $\boldsymbol{H}'(t)$ describes the interaction between the laser field and the molecular system.

Within the Born–Oppenheimer approximation, the Hamiltonian $\boldsymbol{H}_0$ is separated into electronic and nuclear motion parts. The time-independent Schrödinger equation for the nuclear motion part can be expressed as follows:

$$\left[-\frac{1}{2\mu}\frac{\partial^2}{\partial R^2} + \frac{j(j+1)}{2\mu R^2} + V_n(R)\right]\psi_\nu^n(R)Y_j(\theta) = E_{\nu j}^n \psi_\nu^n(R) Y_j(\theta). \tag{6}$$

Here, R denotes the internuclear distance, $V_n(R)$ is the adiabatic potential energy curve of the nth state, and $Y_j(\theta)$ represents the spherical harmonic functions, where j is the rotational quantum number. For the calculation of the vibrational wavefunction, we use a box with an internuclear distance R ranging from 0 to 40 a.u. to avoid spurious wavepacket reflections at the boundaries. Therefore, the eigenstates $|n\nu j\rangle = \psi_\nu^n(R)Y_j(\theta)$ possess eigenenergies $E_{\nu j}^n$. Note that each electronic state n corresponds to a distinct potential energy curve.

The Hamiltonian $\boldsymbol{H}'(t)$ is defined as

$$\boldsymbol{H}'(t) = \boldsymbol{D}_{n'n}(R)\cdot\boldsymbol{E}(t). \tag{7}$$

Here, $\boldsymbol{D}_{n'n}(R)$ is the dipole moment operator between the n'th and nth electronic states, and $\boldsymbol{E}(t)$ denotes the laser field vector. For $n = n'$, this interaction leads to molecular vibrational and rotational excitation as well as the Stark shift induced by the field. For $n \neq n'$, the time-dependent evolution of this interaction results in transitions between electronic states, including single- and multi-photon transitions as well as resonant and non-resonant Raman processes.

If the laser field is treated as a perturbation and laser-induced electronic-state transitions are neglected, based on Eq. (1), Eq. (7) can be approximated as

$$\begin{aligned}\boldsymbol{H}'(t) &= \sum_{n\neq 0}\frac{\langle 0|\boldsymbol{D}\cdot\boldsymbol{E}(t)|n\rangle\langle n|\boldsymbol{D}\cdot\boldsymbol{E}(t)|0\rangle}{E_0 - E_n}\\ &= -\frac{1}{2}\left[(\alpha_\parallel(R)-\alpha_\perp(R))\cos^2\theta+\alpha_\perp(R)\right]E^2(t),\end{aligned} \tag{8}$$

where θ is the angle between the laser polarization and the internuclear axis of the molecule, and $\alpha_\parallel(R)$ and $\alpha_\perp(R)$ are the parallel and perpendicular components of the polarizability, respectively.

According to the Schrödinger equation, the time-dependent evolution of a quantum wave packet satisfies

$$\Psi(R,\theta,t) = \mathrm{e}^{-\mathrm{i}\boldsymbol{H}t}\Psi(R,\theta,0), \tag{9}$$

where $\mathrm{e}^{-\mathrm{i}\boldsymbol{H}t}$ is the time-evolution operator. By introducing small time intervals $\mathrm{d}t$, the full time-dependent wave packet is obtained through iterative propagation at each time step:

$$\Psi(R,\theta,t+\mathrm{d}t) = \mathrm{e}^{-\mathrm{i}\boldsymbol{H}\mathrm{d}t}\Psi(R,\theta,t)+O(\mathrm{d}t^2). \tag{10}$$

Using the second-order split-operator method[41–43] combined with a Taylor expansion, the time-dependent evolution operator of the wave packet can be written as

$$\begin{aligned}&\mathrm{e}^{-\mathrm{i}\boldsymbol{H}\mathrm{d}t} = \mathrm{e}^{-\frac{\mathrm{i}}{2}\boldsymbol{H}_0\mathrm{d}t}\,\mathrm{e}^{-\mathrm{i}\boldsymbol{H}'\mathrm{d}t}\,\mathrm{e}^{-\frac{\mathrm{i}}{2}\boldsymbol{H}_0\mathrm{d}t},\\ &\mathrm{e}^{-\mathrm{i}\boldsymbol{H}'\mathrm{d}t} = 1-\mathrm{i}\boldsymbol{H}'\mathrm{d}t-\frac{\boldsymbol{H}'^2\mathrm{d}t^2}{2}+\frac{\mathrm{i}\boldsymbol{H}'^3\mathrm{d}t^3}{6}+\cdots.\end{aligned} \tag{11}$$

Setting the eigenstates $|n\nu j\rangle$ of the isolated molecule as basis functions, we obtain

$$H'_{n'\nu'j',n\nu j}(t) = \langle\nu' j'|\boldsymbol{D}_{n'n}(R)\cdot\boldsymbol{E}(t)|\nu j\rangle. \tag{12}$$

In Eq. (12), if we only consider the three electronic states ($\mathrm{X}^1\Sigma_\mathrm{g}^+$, $\mathrm{B}^1\Sigma_\mathrm{u}^+$, and $\mathrm{C}^1\Pi_\mathrm{u}$), the matrix elements of the parallel and perpendicular transitions can be expressed as $\langle\nu' j'|D_{\mathrm{X,B}}(R)\cos\theta|\nu j\rangle E(t)$ and $\langle\nu' j'|D_{\mathrm{X,C}}(R)\sin\theta|\nu j\rangle E(t)$, respectively. Additionally, for the non-resonant Raman processes, the matrix element is expressed as

$$\begin{aligned}H'_{0\nu'j',0\nu j}(t) = &-\frac{1}{2}\langle\nu' j'|[\alpha_\parallel(R)-\alpha_\perp(R)]\cos^2\theta\\ &+\alpha_\perp(R)|\nu j\rangle E^2(t).\end{aligned} \tag{13}$$

Further, $H'^2_{n'\nu'j',n\nu j}(t)$, $H'^2_{0\nu'j',0\nu j}(t)$, $H'^3_{n'\nu'j',n\nu j}(t)$, and $H'^3_{0\nu'j',0\nu j}(t)$ are calculated from $H'_{n'\nu'j',n\nu j}(t)$, $H'_{0\nu'j',0\nu j}(t)$, and corresponding matrix operations. After determining the molecular initial electronic–vibrational–rotational state and obtaining the matrix elements of the time-evolution operator in the eigenbasis of $\boldsymbol{H}_0$, we can carry out the time-dependent simulation of laser-induced molecular dynamics. Notably, although the Taylor expansion method cannot strictly guarantee the normalization of the wave-function norm, by reducing the step size $\mathrm{d}t$ and increasing the expansion order, its influence on the norm can be kept below 10^{-4}.

In our simulations, a linearly polarized electric field is applied, mathematically expressed as

$$\boldsymbol{E}(t) = E_0\sin^2\left(\frac{\pi t}{\tau}\right)\sin(\omega t+\phi)\,\boldsymbol{e}_z, \tag{14}$$

where E_0 represents the peak field amplitude, ω denotes the carrier frequency, τ refers to the pulse duration, ϕ is the carrier-envelope phase, and $\boldsymbol{e}_z$ corresponds to the major polarization axis. All simulations employ a $\tau = 60$ fs laser pulse with the carrier-envelope phase fixed at $\phi = \pi/2$.

3. Numerical results and discussion

Figure 1(a) shows the potential energy curves of 90 electronic states, including 30 $\mathrm{X}^1\Sigma_\mathrm{g}^+$ states, 30 Σ_u^+ states, and 30 Π_u states. The energy levels and dipole transition matrix elements between the ground state and the excited states at the equilibrium geometry of H_2 are listed in Table 1. Using quantum perturbation theory as given in Eq. (4), the parallel and perpendicular polarizabilities are calculated to be 6.83 and 5.42, respectively. After accounting for the vibrational distribution of the ground-state H_2 molecule, the corrected values become 7.20 and 5.40, which are in good agreement with the reference data from the National Institute of Standards and Technology (NIST),[44] reporting components of 7.43 and 5.38.

Figures 1(b) and 1(c) show the time-dependent populations of the 90 electronic states under an 800 nm, 50 TW/cm^2 laser pulse. The results indicate that the maximum populations of the low-lying excited states $\mathrm{B}^1\Sigma_\mathrm{u}^+$ and $\mathrm{C}^1\Pi_\mathrm{u}$ are on the order of 10^{-3}, while the population of the highest excited states

only reaches about 10^{-10}. The time-dependent rotational energy shown in Fig. 1(d) further demonstrates that the number of included excited states has a pronounced influence on the simulation results, and at least 36 states are required for convergence.

Table 1. Excited state energy levels of 30 Σ_u^+ and Π_u symmetries and transition dipole moments (in a.u.) with ground H_2 at the equilibrium position. The first and second columns represent the energy levels of 30 excited states Σ_u^+ and Π_u, while the third and fourth columns correspond to the transition dipole moments from the ground state $X^1\Sigma_g^+$ to these 30 excited states Σ_u^+ and Π_u.

Σ_u^+	Π_u	$X^1\Sigma_g^+ \to \Sigma_u^+$	$X^1\Sigma_g^+ \to \Pi_u$
−0.69714	−0.67937	0.96545	0.69788
−0.62458	−0.52217	0.34609	0.89624
−0.58624	−0.5142	−0.50175	0.47867
−0.52397	−0.37718	0.19677	−0.00184
−0.51723	0.05206	6.38149×10^{-5}	−0.00346
−0.45922	0.11206	−0.50502	0.05232
−0.3069	0.15254	0.44263	−0.0445
−0.26974	0.19579	0.00214	0.01167
−0.02857	0.20683	−0.02841	0.00698
0.04387	0.24328	0.01142	6.26411×10^{-4}
0.05665	0.2621	-6.78744×10^{-5}	0.01963
0.08646	0.28666	-6.31768×10^{-4}	0.02435
0.14742	0.31716	−0.04243	−0.01527
0.16937	0.3582	0.01466	−0.0013
0.20701	0.36808	−0.00898	0.00399
0.20799	0.39532	−0.03487	0.00481
0.24795	0.40417	−0.01284	-1.45216×10^{-4}
0.27783	0.42494	0.02109	−0.00251
0.2946	0.43319	−0.00236	0.0083
0.30707	0.44266	−0.01454	0.00243
0.33247	0.45345	−0.03207	−0.0019
0.35886	0.46617	-9.21034×10^{-4}	0.00318
0.36159	0.48842	-7.22618×10^{-4}	0.01213
0.37478	0.50029	−0.0137	0.00195
0.39028	0.50251	0.01376	−0.00844
0.39352	0.50861	0.00367	0.00852
0.41993	0.5253	0.00266	−0.00115
0.4283	0.52852	0.00347	−0.01092
0.42955	0.53919	0.00234	−0.00214
0.44267	0.55199	0.00376	−0.00286

In this work, a systematic comparison is conducted between the rotational dynamics driven by classical-field-approximated electronic dipole transitions and non-resonant Raman processes in neutral H_2 molecules, with a particular focus on the wavelength-dependent behavior under laser fields of different wavelengths. Time-dependent quantum dynamical simulations are performed for multiple electronic and rotational states, with the initial rotational quantum number set to $j = 0$, and calculations including 20 rotational states.

First, to validate the accuracy of the present time-dependent quantum wave packet propagation method, we analyze the temporal evolution of the total population. As shown in Fig. 2, under specified conditions (laser intensity: 50 TW/cm^2, laser wavelength: 800 nm), the total population exhibits a slight temporal drift, which is attributed to the non-unitary nature of the Taylor-expanded time-evolution operator. Our error analysis shows normalization coefficient errors of 10^{-3} and 10^{-4} for time steps (dt) of 0.3085 a.u. and 0.1028 a.u., respectively. Importantly, computational reliability is confirmed by achieving an error as low as 10^{-5} with the implemented time step of d$t = 0.0031$ a.u.

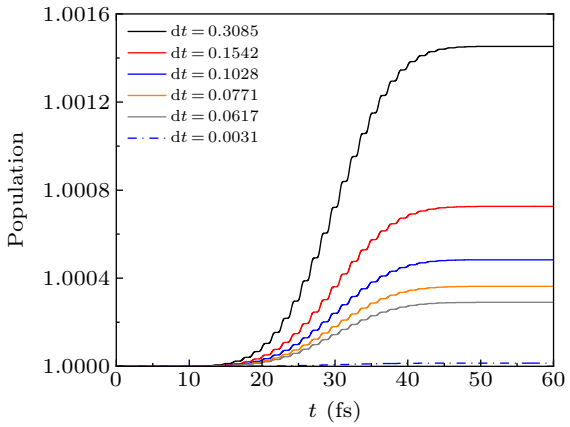


Fig. 2. Temporal evolution of the total population under different time steps for a laser intensity of 50 TW/cm^2 and a wavelength of 800 nm.

For the investigation of wavelength-dependent dynamics, wavelengths of 273 nm, 455 nm, and 800 nm are selected, with 273 nm and 455 nm specifically chosen to facilitate three-photon and five-photon resonances from the ground $X^1\Sigma_g^+$ state to the $B^1\Sigma_u^+/C^1\Pi_u$ states, respectively. At a laser intensity of 50 TW/cm^2, the dynamics driven by distinct photon processes at different wavelengths are investigated, as illustrated in Fig. 3. All 90 electronic states are included in the simulation; the three lowest states ($X^1\Sigma_g^+$, $B^1\Sigma_u^+$, and $C^1\Pi_u$) are mainly considered to illustrate the contributions of electronic excitation and non-resonant Raman processes to molecular rotational dynamics.

Figures 3(a)–3(c) depict the time-dependent population evolution of the ground state $X^1\Sigma_g^+$ (black solid line), excited state $B^1\Sigma_u^+$ (blue solid line), and $C^1\Pi_u$ (red solid line). From these results, we observe that regardless of the laser wavelength, under the classical-field approximation, the electronic states are all excited and reach similar peak populations of approximately 0.5%–1%. After the three-photon resonant laser (273 nm) ends, the total population of the excited states can still reach 0.25%. By contrast, following the five-photon resonant laser (455 nm), only about 0.05% of H_2 molecules are promoted to the excited states. For the 800 nm non-resonant laser, the excited-state population is only about 10^{-7}.

Figures 3(d)–3(f) present the time-dependent population distributions of rotational quantum numbers for ground-state H_2 within the classical-field-approximated electronic dipole transition framework. These rotational populations exhibit a clear wavelength dependence, with lower populations in higher rotational states j as the wavelength increases. These higher rotational states arise from multi-photon resonant Ra-

man processes between the ground and excited states. Specifically, the three-photon resonant Raman process corresponds to $\Delta j = \pm 6$, while the five-photon resonant Raman process corresponds to $\Delta j = \pm 10$. The non-resonant Raman process contributes only $\Delta j = \pm 2$, with the final rotational populations distributed among $j = 0$, 2, and 4. The results in Figs. 3(d) and 3(e) demonstrate that under resonant laser excitation, both non-resonant and resonant Raman processes significantly contribute to rotational excitation. Although the populations of highly rotationally excited states are small, their contribution to the total rotational energy may be significant, since molecular rotational energy scales as $j(j+1)$.

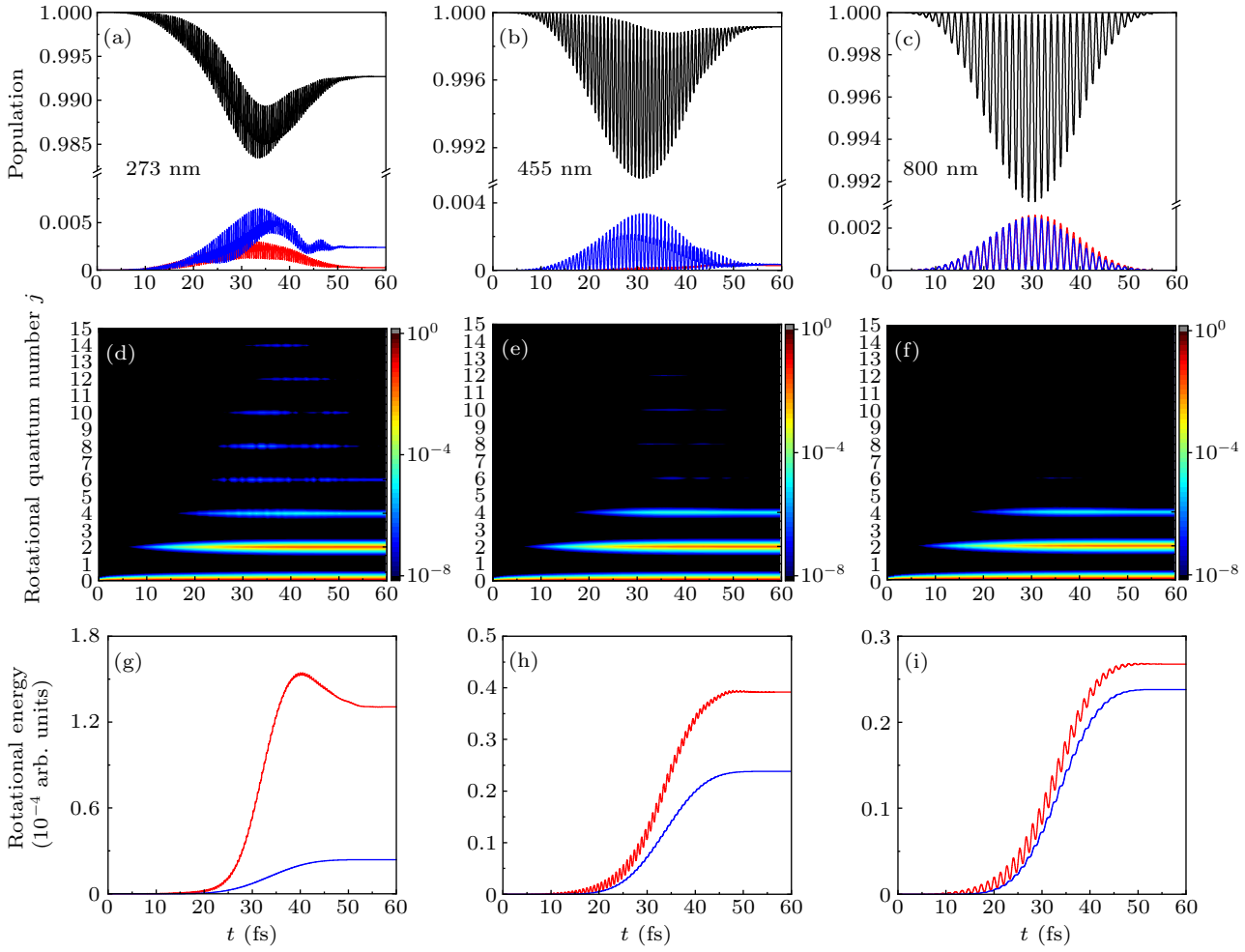


Fig. 3. (a)–(c) Time-dependent population evolution of the ground state $X^1\Sigma_g^+$ (black solid line), and the excited states $B^1\Sigma_u^+$ (blue solid line) and $C^1\Pi_u$ (red solid line). (d)–(f) Distributions of the time-dependent rotational quantum number j for the ground state $X^1\Sigma_g^+$. (g)–(i) Time-dependent rotational energy of ground H_2 calculated using the present TDQWPM method (red solid line) and the non-resonant Raman model (blue solid line).

Consequently, the time-dependent evolution of the rotational energy exhibits pronounced wavelength-dependent behavior, as shown in Figs. 3(g)–3(i). In these figures, the rotational energy populations are represented by red solid lines (present TDQWPM calculations) and blue solid lines (considering only non-resonant Raman processes). At a wavelength of 273 nm, the final rotational energies obtained from these two approaches differ by approximately a factor of seven, from 2.37987×10^{-5} a.u. to 1.30604×10^{-4} a.u. Since the present TDQWPM calculations include both non-resonant Raman processes and resonant electronic transitions, this sevenfold difference indicates that resonant electronic transitions play a decisive role in the rotational excitation of molecules. For 455 nm, the contributions of non-resonant and resonant processes are comparable. For 800 nm, the differences between the two calculations may arise from the limited completeness of the 90 electronic states or minor contributions from electronic state transitions, considering that the total excited-state population reaches only 0.05% at peak laser intensity.

After establishing the coexistence of resonant electronic excitation and non-resonant Raman processes in laser-neutral molecule interactions, the next challenge is to obtain accurate time-dependent excited-state populations induced by resonant electronic excitation within the classical field approximation. In previous studies, excited-state populations directly obtained from simulations were generally assumed to represent the actual populations. However, as shown in Figs. 3(a)–3(c), cal-

culations at different wavelengths yield similar excited-state populations at peak laser intensity, despite significant differences in the contributions from resonant electronic excitation. To clarify this issue, we analyze the photoelectron angular distributions of molecules irradiated by an 800 nm laser. By examining how neutral-to-excited-state transitions followed by ionization affect these angular distributions, we determine the correct excited-state populations.

Figure 4 presents two types of time-dependent populations of $B^1\Sigma_u^+$, used to investigate the contribution of the excitation-then-ionization process to H_2 molecular ionization. The red solid curve (Model-1) represents the direct computational results obtained using the TDQWPM method, assuming that molecules occupying the simulated excited state at any time may undergo tunneling ionization. In contrast, the blue solid curve (Model-2) represents the populations measured when the laser field is zero. We propose that only the population remaining in the excited state after one full laser field oscillation ($E = 0$) corresponds to genuine photoexcitation events. Transient populations that increase and then decrease during laser oscillations arise from either resonant or non-resonant Raman processes, which do not contribute to subsequent ionization.

Based on this analysis, we employ the molecular Ammosov–Delone–Krainov (MO-ADK) theory[45,46] to calculate ionization yields and orientation dependencies using

$$Y(t) = \iiint P_i(t)p_1(R,\theta,t)\sin\theta\,\mathrm{d}R\,\mathrm{d}\theta\,\mathrm{d}t, \tag{15}$$

$$P'(\theta) = \iint P_i(t)p_1(R,\theta,t)\,\mathrm{d}R\,\mathrm{d}t. \tag{16}$$

Here, $Y(t)$ represents the ionization yield, $P'(\theta)$ denotes the orientation dependence, $P_i(t)$ corresponds to the time-evolving populations of the two mechanisms, and $p_1(R,\theta,t)$ is the ionization probability calculated from MO-ADK theory. The MO-ADK parameters used for the $X^1\Sigma_g^+$, $B^1\Sigma_u^+$, and $C^1\Pi_u$ states are listed in Table 2.

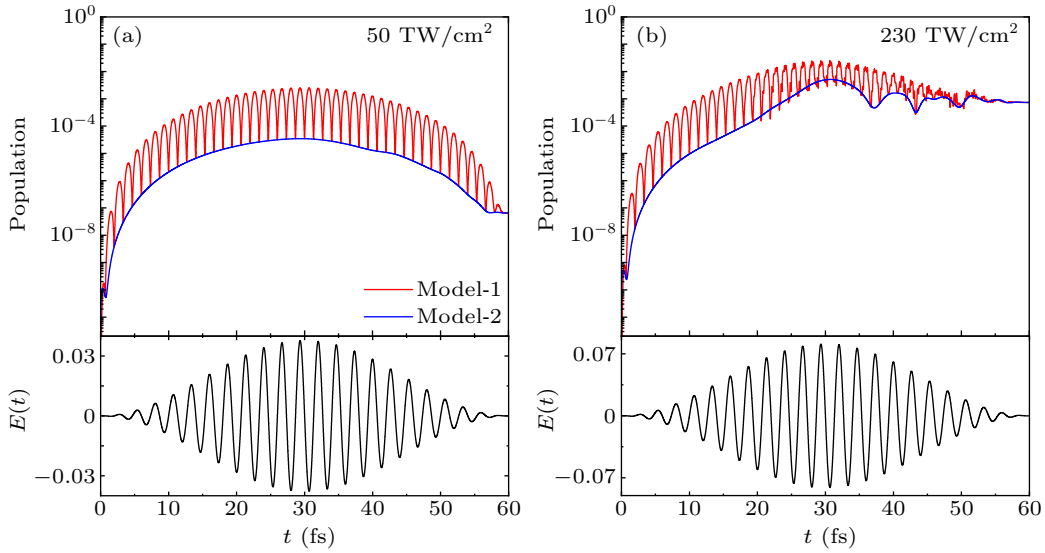


Fig. 4. Time-dependent populations of the excited state $B^1\Sigma_u^+$ under different laser field intensities. (a) and (b) correspond to laser intensities of 50 TW/cm^2 and 230 TW/cm^2, respectively. In both panels, the black solid curve represents the laser pulse, the red solid curve shows Model-1 results obtained using the present TDQWPM method, and the blue solid curve represents Model-2, corresponding to the connected data points of excited-state populations at zero laser field intensity.

Table 2. The C_l coefficients of $X^1\Sigma_g^+$, $B^1\Sigma_u^+$ and $C^1\Pi_u$ with ground H_2 at the equilibrium position. For Σ orbital, $m = 0$ and Π orbital, $m = 1$. The binding energies are also listed.

Symmetry	Binding energy (eV)	C_l		
$X^1\Sigma_g^+$	15.65	C_{0m}	C_{2m}	C_{4m}
		1.42838	0.08538	0.00141
$B^1\Sigma_u^+$	3.36	C_{1m}	C_{3m}	C_{5m}
		0.40586	0.01069	0.00025
$C^1\Pi_u$	3.03	C_{1m}	C_{3m}	C_{5m}
		0.03771	0.00180	0.00001

Due to the significantly lower ionization potential of H_2 excited states compared to the ground state, even though the excited-state population remains orders of magnitude smaller than that of the ground state at any moment, it can still contribute significantly to strong-field ionization. Figure 5 systematically illustrates the ionization dynamics of the two mechanisms under a laser intensity of 230 TW/cm^2. In Figs. 5(a) and 5(f), the time-dependent ionization yields of the ground state $X^1\Sigma_g^+$ (black), excited state $B^1\Sigma_u^+$ (red), and excited state $C^1\Pi_u$ (blue) are presented. Interestingly, Fig. 5(a) (Model-1) indicates that the probability of tunneling ionization following excitation from the ground state to $B^1\Sigma_u^+$ actually exceeds that of direct tunneling ionization from the ground state. Moreover, the probability for the $X^1\Sigma_g^+$ to $C^1\Pi_u$ excitation followed by tunneling ionization is comparable to direct ground-state tunneling ionization. This result significantly overestimates the contribution of excited states to ionization

under the laser parameters of 230 TW/cm^2 and 800 nm, where the Keldysh parameter γ[47] is less than 1.

The total ionization angular distribution shown in Fig. 5(e), calculated based on the rotational wave functions and ionization angular distributions of the $X^1\Sigma_g^+$, $B^1\Sigma_u^+$, and $C^1\Pi_u$ states, also exhibits significant discrepancies with experimental measurements (gray dashed line in Fig. 5(j)). Notably, the theoretical results exhibit pronounced minima at 90°/270°, primarily arising from contributions of the $B^1\Sigma_u^+$ state, which contradict experimental observations. These discrepancies demonstrate that the population variations in molecular excited states induced by either resonant or non-resonant Raman processes under the classical field approximation do not correspond to genuine photo-excitation processes and should not be included in photo-excitation-ionization events.

After removing these unphysical contributions, we adopt the blue solid curve (Model-2) in Fig. 4(b) as the time-dependent population of the excited state to recalculate the respective contributions of direct ground-state tunneling ionization and excitation-then-ionization processes to H_2 molecular ionization. As anticipated, the contribution from excitation-then-ionization decreases to approximately 14.1%. The resulting total ionization angular distribution, shown in Fig. 5(j), exhibits excellent agreement with experimental measurements by Staudte *et al.*[48] and theoretical predictions by Tong *et al.*[45] and Zhao *et al.*[46]

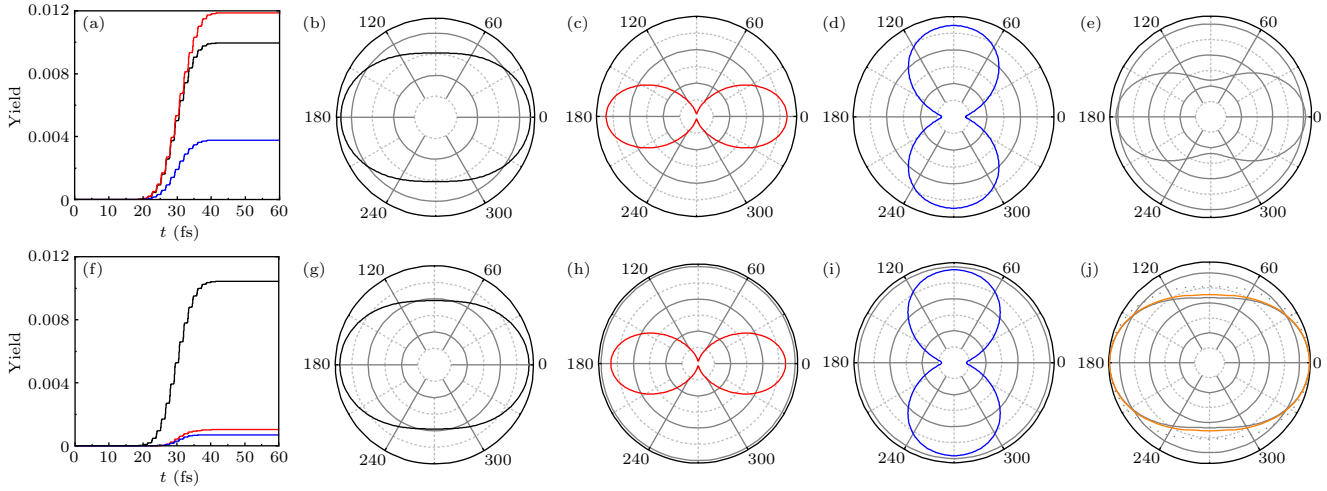


Fig. 5. Ionization yields and angular distributions of neutral H_2 molecules for different electronic states at 230 TW/cm^2. (a) and (f) show the ionization yields of Model-1 and Model-2, respectively. In these panels, the black solid line corresponds to direct tunneling ionization from the ground state $X^1\Sigma_g^+$, while the red and blue solid lines represent contributions from $X^1\Sigma_g^+$-to-$B^1\Sigma_u^+$ and $X^1\Sigma_g^+$-to-$C^1\Pi_u$ excitations followed by tunneling ionization, respectively. (b) and (g) present the ionization angular distributions of Model-1 and Model-2 for the ground state $X^1\Sigma_g^+$, (c) and (h) correspond to $B^1\Sigma_u^+$, and (d) and (i) correspond to $C^1\Pi_u$. (e) and (j) show the total ionization angular distribution, summing contributions from $X^1\Sigma_g^+$, $B^1\Sigma_u^+$, and $C^1\Pi_u$. In panel (j), the gray dashed line represents experimental measurements[47], and the orange solid line denotes theoretical calculations by Zhao *et al.*[46,48].

4. Conclusion

In summary, we have developed a fully time-dependent quantum wave packet propagation method that accounts for dipole transitions among multiple electronic states, enabling a unified treatment of resonant electronic transitions, resonant Raman processes, and non-resonant Raman processes. Using H_2 as a prototypical system, this approach has been employed to investigate rotational excitation and strong-field ionization dynamics. Through systematic comparisons with experimental measurements and other theoretical calculations, we draw two principal conclusions:

(i) Electronic transitions, resonant Raman processes, and non-resonant Raman processes inherently coexist. Even under 800 nm non-resonant laser irradiation at 230 TW/cm^2, the excitation-then-ionization pathway contributes approximately 14.1% to the total ionization yield.

(ii) Population variations in molecular excited states induced by either resonant or non-resonant Raman processes under the classical field approximation do not correspond to genuine photo-excitation events and should not contribute to photo-excitation-ionization processes.

Moreover, the developed methodology is readily extendable to more complex molecular fragmentation dynamics, particularly for processes involving multiple charge states, a large number of electronic states, and vibrational and rotational degrees of freedom.

Acknowledgments

This work was supported by the National Key Research and Development Program of China (Grant No. 2022YFA1602502) and the National Natural Science Foundation of China (Grant No. 12450404).

References

[1] Itatani J, Levesque J, Zeidler D, Niikura H, Pépin H, Kieffer J C, Corkum P B and Villeneuve D M 2004 *Nature* **432** 867

[2] Zhai C, Zhu X, Lan P, Wang F, He L X, Shi W J, Li Y, Li M, Zhang Q B and Lu P X 2017 *Phys. Rev. A* **95** 033420

[3] Zhai C Y, He L X, Lan P F, Zhu X S, Li Y, Wang F, Shi W J, Zhang Q B and Lu P X 2016 *Sci. Rep.* **6** 23236

[4] Liu K and Barth I 2016 *Phys. Rev. A* **94** 043402

[5] Baker S, Robinson J S, Haworth C A, Teng H, Smith R A, Chirilă C C, Lein M, Tisch J W G and Marangos J P 2006 *Science* **312** 424

[6] Mercer I, Mevel E, Zerne R, L' Huillier A, Antoine P and Wahlström C G 1996 *Phys. Rev. Lett.* **77** 1731

[7] Hay N, Velotta R, Lein M, Nalda R D, Heesel E, Castillejo M and Marangos J P 2002 *Phys. Rev. A* **65** 053805

[8] Yuan K J and Bandrauk A D 2018 *Phys. Rev. A* **98** 023413

[9] Zuo T and Bandrauk A D 1995 *Phys. Rev. A* **52** R2511

[10] Posthumusy J H, Gilesy A J, Thompsony M R, Shaikhz W, Langley A J, Frasinski L J and Codling K 1996 *J. Phys. B: At. Mol. Opt. Phys.* **29** L525

[11] Seideman T 1995 *J. Chem. Phys.* **103** 7887

[12] Seideman T 1999 *Phys. Rev. Lett.* **83** 4971

[13] Yun S J, Kim C M, Lee J and Nam C H 2012 *Phys. Rev. A* **86** 051401

[14] Giusti-Suzor A, He X, Atabek O and Mies F H 1990 *Phys. Rev. Lett.* **64** 515

[15] Posthumus J H 2004 *Rep. Prog. Phys.* **67** 623

[16] Ergler T, Rudenko A, Feuerstein B, Zrost K, Schröter C D, Moshammer R and Ullrich J 2006 *Phys. Rev. Lett.* **97** 193001

[17] Chelkowski S, Bandrauk A D, Staudte A and Corkum P B 2007 *Phys. Rev. A* **76** 013405

[18] Stapelfeldt H and Seideman T 2003 *Rev. Mod. Phys.* **75** 543

[19] Lemeshko M and Friedrich B 2010 *J. Phys. Chem. A* **114** 9848

[20] Koch C P, Lemeshko M and Sugny D 2019 *Rev. Mod. Phys.* **91** 035005

[21] Xu T, Ma J P, Hu X Q, Tang Y S, Pei S Q, Jia C C, Wu Y and Wang J G 2025 *Chin. Phys. B* **34** 053301

[22] Atkins P W and Friedman R S 2001 *Molecular Quantum Mechanics*, third edition (Oxford: Oxford University Press)

[23] Martinez T J, Ben-Nun M and Levine R D 1996 *J. Phys. Chem.* **100** 7884

[24] Abanador P M and Thumm U 2020 *Phys. Rev. A* **102** 053114

[25] Azarm A, Song D, Liu K, Hosseini S, Teranishi Y, Lin S H, Xia A, Kong F and Chin S L 2011 *J. Phys. B: At. Mol. Opt. Phys.* **44** 085601

[26] Sanz-Vicario J L, Bachau H and Martín F 2006 *Phys. Rev. A* **73** 033410

[27] Martín F, Fernández J, Havermeier T, Foucar L, Weber T, Kreidi K, Schoöffler M, Schmidt L, Jahnke T, Jagutzki O, Czasch A, Benis E P, Osipov T, Landers A L, Belkacem A, Prior M H, Schmidt-Boöcking H, Cocke C L and Dörner R 2007 *Science* **315** 629

[28] Sturm F P, Tong X M, Palacios A, Wright T W, Zalyubovskaya I, Ray D, Shivaram N, Martín F, Belkacem A, Ranitovic P and Weber T 2017 *Phys. Rev. A* **95** 012501

[29] Ranitovic P, Hoglea C W, Rivièrec P, Palacios A, Tong X M, Toshima N, González-Castrillo A, Martin L, Martín F, Murnane M M and Kapteyn H 2014 *Proc. Natl. Acad. Sci. USA* **111** 912

[30] Sun T, Zhao L, Liu Y, Guo J, Lv H and Xu H F 2023 *Phys. Rev. A* **108** 013120

[31] Borisova G D, Belda P B, Hu S Y, Birk P, Stoo V, Hartmann M, Fan D, Moshammer R, Saenz A, Ott C and Pfeifer T 2024 *Phys. Rev. R* **6** 033326

[32] Bucksbaum P H, Zavriyev A, Muller H G and Schumacher D W 1990 *Phys. Rev. Lett.* **64** 1883

[33] He F, Becker A and Thumm U 2008 *Phys. Rev. Lett.* **101** 213002

[34] Nubbemeyer T, Eichmann U and Sandner W 2009 *J. Phys. B: At. Mol. Opt. Phys.* **42** 134010

[35] Zohrabi M, McKenna J, Gaire B, Johnson N G, Carnes K D, De S, Bocharova I A, Magrakvelidze M, Ray D, Litvinyuk I V, Cocke C L and Ben-Itzhak I 2011 *Phys. Rev. A* **83** 053405

[36] Magrakvelidze M, Aikens C M and Thumm U 2012 *Phys. Rev. A* **86** 023402

[37] Wu J, Schmidt L Ph H, Kunitski M, Meckel M, Voss S, Sann H, Kim H, Jahnke T, Czasch A and Dörner R 2012 *Phys. Rev. Lett.* **108** 183001

[38] Zhang W B, Li Z C, Lu P F, Gong X C, Song Q Y, Ji Q Y, Lin K, Ma J Y, He F, Zeng H P and Wu J 2016 *Phys. Rev. Lett.* **117** 103002

[39] Werner H J, Knowles P J, Knizia G, *et al*. 2010 *MOLPRO, a package of ab initio programs*, version 2010.1. See http://www.molpro.net

[40] Dunning T H Jr 1989 *J. Chem. Phys.* **90** 1007

[41] Reinsch M W 2000 *J. Math. Phys.* **41** 2434

[42] Bialynicki-Birula I, Mielnik B and Plebański J 1969 *Annals of Physics.* **51** 187

[43] Feit M D, Fleck J A and Steiger A 1982 *Journal of Computational Physics* **47** 412

[44] *NIST Computational Chemistry Comparison and Benchmark Database*

[45] Tong X M, Zhao Z X and Lin C D 2002 *Phys. Rev. A* **66** 033402

[46] Zhao S F, Jin C, Le A T, Jiang T F and Lin C D 2010 *Phys. Rev. A* **81** 033423

[47] Keldysh L V 1965 *Sov. Phys. JETP.* **20** 1307

[48] Staudte A, Patchkovskii S, Pavičić D, Akagi H, Smirnova O, Zeidler D, Meckel M, Villeneuve D M, Dörner R, Ivanov M Y and Corkum P B 2009 *Phys. Rev. Lett.* **102** 033004